Published in final edited form as:
J Biol Chem. 2007 February 9; 282(6): 4035–4044.

Self-Chaperoning of the Type III Secretion System needle tip proteins IpaD and BipD

Steven Johnson[a,b,†], **Pietro Roversi**[a,†], **Marianela Espina**[c], **Andrew Olive**[c], **Janet E. Deane**[a], **Susan Birket**[c], **Terry Field**[d], **William D. Picking**[c], **Ariel Blocker**[b], **Edouard E. Galyov**[d], **Wendy L. Picking**[c], and **Susan M. Lea**[b,a]

aLaboratory of Molecular Biophysics, Department of Biochemistry, University of Oxford, UK

bSir William Dunn School of Pathology, University of Oxford, UK

cDepartment of Molecular Biosciences, University of Kansas, USA

dDivision of Microbiology, Institute for Animal Health, Compton Laboratory, Berkshire, RG20 7NN, UK

Abstract

Bacteria expressing type III secretion systems (T3SS) have been responsible for the deaths of millions worldwide, acting as key virulence elements in diseases ranging from plague to typhoid fever. The T3SS is composed of a basal body, which traverses both bacterial membranes, and an external needle through which effector proteins are secreted. We report multiple crystal structures of two proteins that sit at the tip of the needle and are essential for virulence; IpaD from *Shigella flexneri* and BipD from *Burkholderia pseudomallei*. The structures reveal that the N-terminal domains of the molecules are intra-molecular chaperones that prevent premature oligomerization, as well as sharing structural homology with proteins involved in eukaryotic actin rearrangement. Crystal packing has allowed us to construct a model for the tip complex that is supported by mutations designed using the structure.

Introduction

Currently, more than 1 million people die *per annum* as a result of T3SS-expressing enteropathogenic bacteria such as *Shigella flexneri*, the causative agent of human bacillary dysentery(1). The T3SS is composed of a basal body, which traverses both bacterial membranes, and an external needle through which effector proteins are secreted(2). During infection, secretion is activated by contact of the tip of the needle complex with host cells(3) resulting in formation of a pore in the host cell membrane that is thought to be contiguous with the needle(4). Other effector proteins are injected through this apparatus directly into the host cell cytoplasm (for a review, see(5)). T3SS-expressing bacteria can be classified into distinct phylogenetic families, both at the sequence level and by their general mechanism of infection (6). The Inv-Mxi-Spa family express T3SS which trigger uptake of bacteria by non-phagocytic cells and includes *S. flexneri* and *Burkholderia pseudomallei*.

Shigella spp. cause bacillary dysentery by invasion of the colonic epithelium(7). Of the *S. flexneri* T3SS effector proteins, IpaB, IpaC and IpaD are essential for invasion(8). IpaB and IpaC have been demonstrated to insert into the host cell membrane, thereby forming the translocation pore(4). Bacteria lacking IpaD are not only incapable of pore insertion and invasion, but also demonstrate impaired effector secretion control(9). IpaD was originally proposed to form a plug in the T3SS with IpaB(3), while more recent data have demonstrated

E-mail: susan.lea@path.ox.ac.uk
† These authors contributed equally to this work.

that its role is more complex(9). Deletions within the N-terminal third of the molecule do not affect invasion of host cells by the bacteria, although the insertion of IpaB/IpaC into membranes is slightly impaired. However, even short deletions (5 residues) in the C-terminus of IpaD completely abolish the invasive phenotype and pore insertion(9). These observations led us to suggest that IpaD may play a role in regulating insertion of the IpaB/IpaC translocon pore from the tip of the *S. flexneri* needle(9,10). Our recent data conclusively demonstrate IpaD is at the tip of intact T3SS embedded in the bacterial membranes and on isolated needles even prior to secretion induction(11). Similarly, the functional homologue in *Y. pestis*, LcrV, has also recently been localized to the tip of the needle and is required for pore formation(12).

B. pseudomallei causes melioidosis in humans, a disease endemic in Southeast Asia and Northern Australia. This disease presents in a variety of ways from subacute and chronic suppurative infections to a rapidly fatal septicaemia(13). *B. pseudomallei* infection is dependent on a T3SS which contains clear homologues of IpaB/C/D termed BipB/C/D(14). The overall sequence identity between IpaD and BipD is only 26 %, however, with most of the conserved residues residing in the C-terminal quarter of the sequence (Fig. 1).

We have recently determined the crystal structure of MxiH, the *S. flexneri* needle subunit, and assembled a molecular model of a T3SS needle by docking it into our 16 Å electron microscopy (EM) reconstruction of the *S. flexneri* needle(15,16). As part of an ongoing study into the interactions of the T3SS with host cells, we have now crystallized and determined the structures of IpaD and BipD. Their three-dimensional structures, in conjunction with the structure of the MxiH needle and other tip proteins such as LcrV(17), significantly increase our understanding of these complex biological machines.

Methods

IpaD crystal structure determination

Protein preparation and crystallization were described previously(18). The positions of 8 Se atoms in the SeMet labelled crystal from 4 (CF-4) were obtained by analyzing the measured anomalous differences using SHELXC/D(19) within the suite of computer programs autoSHARP(20). Initial phases were calculated with the program SHARP(21) using the data from a native crystal and a MAD dataset from a SeMet-derivative (3 peak wavelength datasets and 1 remote wavelength dataset). Analysis of the Log-likelihood gradient maps in SHARP revealed two more Se sites which were added to the phasing job and the SHARP phases were extended to 2.8 Å by solvent flattening in SOLOMON. See Supplementary Table 1 for phasing statistics. Non-crystallographic symmetry (NCS) twofold averaging was carried out in RESOLVE(22) using the positions of the Se to calculate an initial NCS operator. An initial helical model was built in the program CCP4-ARP/wARP-HelixBuild(23) using these phases, and sidechains were remodelled to the IpaD sequence in Xfit(24), using the Se positions as sequence markers. The twofold NCS operator was used to group the helices into 2 monomers, and two copies of one such monomer were then located by Molecular Replacement in both CF-1 and CF-2(18) using CCP4-PHASER(23). Six-fold cross-crystal averaging between the three crystal forms was performed using CCP4-DMMULTI(23) and produced a 2.1 Å map in CF-2 which enabled automated building in CCP4-ARP/wARP (270 residues built, of which 227 were docked into sequence). Alternate cycles of refinement using Buster-TNT(25) and manual rebuilding in Xfit led to the final model in CF-2 of residues 144-314 for copy A and 133-319 for copy B. The complete model from CF-2 was used to guide manual building of models in CF-4 (residues 124-177 and 183-322 in copy A and 123-328 in copy B) with a combination of molecular replacement phases and density modification in DM and DMMULTI. Finally, the N-terminal domain of IpaD (residues 39-130) were built in CF-1 using Buster-TNT to model the missing atoms during the initial stages of refinement of the incomplete structure. Once the residues defining helices α1 and α2 were built, this model was

used to phase the anomalous differences of a Hg-soaked CF-1 crystal in CCP4-FFT(23), and locate 2 Hg ions, which in turn were used to improve the CF-1 phases in SHARP, followed by solvent-flattening in SOLOMON to 2.8 Å. The SHARP-SOLOMON phases were combined with the Buster-TNT phases and 4-fold averaging between CF-1 and CF-2 was repeated, again using DMMULTI. These maps allowed manual building of the final model for CF-1 of residues 39-322 for copy A, and for copy B. All pictures were generated using PyMOL(26).

BipD crystal structure determination

Protein preparation and crystallization were described previously(27). The positions of 2 Pt ions were obtained by analyzing the anomalous differences of a K_2PtCl_4 soaked derivative of the $P2_12_12$ crystal form using SHELXC/D(19) in autoSHARP(20). Initial 3.0 Å phases were calculated with the program SHARP(21) using the single isomorphous replacement with anomalous scattering (SIRAS) method with data from a native crystal and the Pt-derivative. After addition of the data for a SeMet derivative crystal, analysis of the Log-likelihood gradient maps in SHARP revealed 10 Se sites; SOLVE/RESOLVE(22), extended these MIRAS SHARP phases to 2.7 Å and autobuilt and docked in sequence BipD residues 49-69, 77-95, 99-110, 128-166, 180-197, 201-212, 232-238 and 243-301 in at least one of the two independent monomers. The autodocked sequence and the Se positions guided the determination of the NCS twofold operator relating chains A and B, and the NCS was then used to fill the gaps in the autobuilt model for either chain. Finally, iterative cycles of manual building in Xfit(24) and Buster-TNT refinement with soft NCS restraints yielded a model for residues 35-110 and 128-301 for both BipD molecules A and B. The $P2_12_12$ model was used to solve the C222 crystal form by Molecular Replacement with the program CCP4-PHASER(23).

Structure superposition

All structure superpositions were carried out using the program CCP4-lsqkab(23) as follows: IpaD onto IpaD, BipD and MxiH using Superpose Topology; IpaD onto FliS (1ORJ-A), YscE (1ZW0-A), α-catenin (1DOV-A), vinculin (1RKC-A) and talin (1SJ7-A) using the residue mapping as defined by the DALI server (28).

Sequence alignment

IpaD was aligned with *Salmonella enterica typhimurium* SipD using ClustalW(29) and with BipD by structure superposition. The sequence alignment was submitted to the ESPript server (30) for graphical representation.

Limited proteolysis

Pure IpaD at 1 mg/ml was incubated with sequencing grade trypsin (Promega, UK) in 20 mM Tris, pH 7.5, 150 mM NaCl. Ratios of trypsin:IpaD (w/w) of 1:50, 1:100, 1:200, 1:500 and 1:5000 were prepared and incubated in a water bath at 37 °C for 1 hour. The reaction was stopped by the addition of 2× SDS-PAGE sample buffer followed by boiling for 5 min. The samples were analysed by SDS-PAGE and sent for N-terminal sequencing (Protein Characterisation Facility, Dept. of Biochemistry, University of Oxford).

The broad-spectrum serine protease subtilisin Carlsberg from *Bacillus licheniformis* (Sigma-Aldrich) was added to IpaD in a 1:5000 (w/w) ratio (enzyme:protein), and incubated at 20 °C for 72 hrs to mimic the conditions under which crystals grew. The digested protein was then applied to a Superdex 200 (HR 10/30) column (GE Biosciences, UK) equilibrated in 20 mM Tris, pH 7.5, 100 mM NaCl, 10 mM DTT. Undigested IpaD was applied to the same column under identical conditions.

Tip localisation of IpaD/BipD/IpaB and Hemolysis assay

S. flexneri were grown to log phase in tryptic soy broth according to established protocols (31). Bacteria were fixed to glass slides or carbon/Formvar coated copper grids. Monoclonal anti-IpaD, rabbit anti-BipD or rabbit anti-IpaB IgG were used to detect IpaD(11), BipD or IpaB (Supplementary Figure 2), respectively. Alexa Fluor 488 goat anti-mouse IgG or Alexa Fluor 568 goat anti-rabbit IgG was used to detect the primary antibody for confocal microscopy while gold-labelled goat anti-mouse IgG or anti-rabbit IgG was used for electron microscopy. Hemolysis assays were performed as described in reference (4).

Results

Structure of IpaD and BipD

The structure of *S. flexneri* IpaD was determined at 3.0 Å by single isomorphous replacement with anomalous scattering (SIRAS), using a selenomethionine derivative and cross-crystal averaging between various crystal forms(18) (Table 1). The electron density (Fig. 2a) allowed building of a model for IpaD residues 39 to 322 (Figs. 1a & 2b). The structure of *B. pseudomallei* BipD was determined at 2.8 Å by multiple isomorphous replacement with anomalous scattering (MIRAS) using K_2PtCl_4 and SeMet derivatives(27) (Table 1). The electron density (Fig. 2c) allowed construction of a model from residues 35-111 and 127-301 (Fig. 1c & 2d).

Despite sharing only 26 % identity at the sequence level, the structures of IpaD and BipD are highly homologous (rmsd = 1.6 Å over 161/283 Cα atoms). Both proteins are characterized by a long helical coiled-coil formed between a helix at the centre of the sequence and a helix at the C-terminus (Fig. 1b). A predominantly helical domain (hereafter termed the N-terminal domain) precedes the first helix of the central coiled-coil, while the sequence encoding a mixed alpha-beta domain (hereafter termed the C-terminal domain) is inserted between the two long helices of the coiled-coil. Two helices from the N-terminal domain (named α1 and α2, see Fig. 1b) fold against one end of the coiled-coil, while two helices from the C-terminal domain (α4 and α6) pack against the other end of the coil. Both molecules therefore comprise two four-helix bundles that share the long coiled-coil. In addition, the N-terminal domain of IpaD contains a helical insertion relative to BipD between α2 and α3 which wraps around the end of the coiled-coil; while BipD contains a less structured insertion relative to IpaD between α1 and α2. In both IpaD and BipD, the C-terminal domain is embellished by a three-stranded anti-parallel β-sheet at the very end of the coil and an insertion of a short α-helix (α5) and two β-strands (βC, βD) between α4 and α6 of the bundle. Despite the conserved topology, the relative orientation of α5-βC-βD compared to the rest of the molecule differs between IpaD and BipD. The C-terminal residues are not visible in any of the structures. These are the residues that have been demonstrated to be essential for binding of IpaD to the tip of the *S. flexneri* needle(11). Disordered termini have been observed in other T3SS(32) and flagellar filament(33) molecules and this feature has been proposed to be important in correct assembly of these structures (33).

N-terminal domain as chaperone

The N-terminal four-helix bundle of IpaD/BipD shows strong structural homology with chaperones of T3SS filament-forming proteins (DALI,(28)). The strongest hit (Z-score = 11.0) is the flagella chaperone FliS (Figure 3a), a four-helix bundle that prevents premature assembly of the flagellum by binding the C-terminal helix of FliC(34). A DALI search using the N-terminal domain of IpaD alone retrieved YscE(35), the putative chaperone of the *Y. pestis* needle component YscF (Fig. 3b). In addition, the structure of CesA, the chaperone of EspA (a protein which forms a helical filament extension to the T3SS needle of *Enteropathogenic Escherichia coli* (*EPEC*)) is also reminiscent of the IpaD/BipD N-terminal domain(32).

During the initial crystallization trials of IpaD we observed a crystal form which grew over a long period of time that was shown by N-terminal sequencing to consist of a truncated form of the protein(18). Incubation of IpaD with increasing concentrations of trypsin resulted in a gradual degradation to a protease resistant core (Fig. 4a) identified by N-terminal sequencing to start at Ile138. The proteolytic sensitivity of the N-terminal domain of IpaD is in agreement with our earlier biophysical characterization of IpaD which demonstrated that the N-terminal domain unfolds at lower temperatures and independently of the rest of the molecule(36).

To date, no specific chaperones for IpaD or BipD have been identified. Our data suggest that the role of the N-terminal domain of IpaD/BipD is to chaperone residues on the coiled-coil involved in interactions with the needle and/or itself. Removal of the N-terminal domain *in silico* results in the exposure of 2100 Å^2 of solvent-accessible surface area(37), including a hydrophobic strip that runs along the face of the two α-helices of the coiled-coil (Fig. 4b). Removal of the N-terminal domain of BipD exposes an even more extended patch (2300 Å^2). All crystals grown with N-terminally truncated IpaD pack in such a way as to bury this patch in crystal contacts. Furthermore, proteolytic removal of the N-terminal domain of IpaD leads to oligomerization in solution. Full length IpaD elutes as an approximately 50 kDa protein during size exclusion chromatography (Figure 4c). Subtilisin treatment, which clips the N-terminal third of the molecule(18), leads the truncated form to elute as an approximately 115 kDa protein, a size consistent with the formation of a tetramer or pentamer.

In addition, the helices of the coiled-coil seem to be constrained by the N-terminal domain (Fig. 4d). In the presence of the N-terminal domain, the coiled-coil is rigid and invariant between the two crystallographically independent molecules in the intact IpaD crystals and the three independent molecules seen in the BipD crystals. In the absence of the N-domain, however, the coiled-coil acquires flexibility, as demonstrated in the four crystallographically independent truncated IpaD molecules. These results represent the first examples of T3SS molecules self-chaperoning.

IpaD/BipD and actin reprogramming

Three of the top five hits against the DALI database using IpaD/BipD as a search model are proteins involved in rearrangements of the actin cytoskeleton; talin(38) (Z-score = 10.8, rmsd = 2.2 Å over 111 Cα atoms), vinculin(39) (Z-score = 10.1, rmsd = 2.3 Å over 106 Cα atoms) and α-catenin(40) (Z-score = 9.0, rmsd = 3.9 Å over 158 Cα atoms) (Supplementary Fig. 1). Furthermore, like IpaD/BipD, these structural homologues are proteins that are characterized by multiple helical bundles which are capable of helical rearrangement. This is significant as bacteria of the *Shigella/Salmonella* family cause membrane ruffling by actin rearrangement in order to invade nonphagocytic cells. A possible role for IpaD/BipD in interfering with host cell actin is examined in the Discussion.

IpaD/BipD at the tip of the needle

We have recently proposed a model by which LcrV, the functional homologue of IpaD/BipD in *Y. pestis*, may oligomerize at the tip of the needle based on homologies between the LcrV and MxiH structures(16). However, although we can immunolabel IpaD on the tip of the *S. flexneri* needle(11), we have been unable to directly visualize a *S. flexneri* tip complex. This is unsurprising as modelling of IpaD/BipD onto the needle in an analogous way to the LcrV results in a structure that would be difficult to visualize at the resolution of our current images, appearing as an extension to the needle, compared with the more bulky LcrV tip (data not shown).

Despite this, one of the IpaD crystal structures (CF-2) does point toward a possible arrangement of IpaD/BipD at the tip. The crystal, which diffracted to 2.1 Å, contains a tightly packed dimer

(Fig. 5a) in which the two copies of the molecule in the asymmetric unit are related by a rotation of 72.2° around the long axis of the molecule and a rise of 4.6 Å, comparable to the parameters defining the 1-start helix of the MxiH needle(16). This dimer buries 1500 $Å^2$ (14%) of the solvent-accessible surface area of each IpaD monomer(37), including the hydrophobic strip that runs along the length of the coiled-coil, and contains two inter-molecular salt-bridges (K151-E229 and E154-K300) involving residues which are solvent exposed in the full length monomer.

The residues involved in forming this contact are clustered in the C-terminal helix, with one face providing half of the binding pocket for another face of the same helix from a neighbouring monomer (Fig. 5b). These residues are the most conserved residues in the *Shigella/Salmonella* family of tip proteins (Fig. 1d). By superposing molecule A onto molecule B, and then again in an iterative fashion, it is possible to build a tightly packed pentamer which buries all of the hydrophobic surfaces in the molecule (Fig. 5c). This pentamer buries 3000 $Å^2$ (28%) of the solvent-accessible surface area of each monomer. Furthermore, the arrangement places the N-terminal helix of the coiled-coil on the outside of the pentamer, thereby allowing the N-domain to be positioned outside of the needle. Supporting the physiological relevance of these interactions, a double mutation that destroys the two salt-bridges involved in the pentamer formation (K151E; E154K) reduces the hemolytic activity to 55.3 ± 3.6 % of that of the wild type bacteria.

One major consequence of the formation of this pentamer is the fact that it is closed, i.e. there is no hole through the centre of the structure. This is consistent with the earlier observations that bacteria lacking IpaD secrete the later effector proteins constitutively(3). However, the observation in the same study that bacteria lacking IpaB display the same phenotype, combined with data showing surface localization of IpaB(41), led to the proposal that IpaD and IpaB form a plug together in the needle(3). Subsequent studies have demonstrated IpaB decorates the surface of *S. flexneri* in a punctate pattern(42) and is associated with the tips of purified needles (A.J.B., manuscript submitted & W.L.P., manuscript submitted). Although there is currently no atomic model of IpaB, it is predicted to contain two long coiled-coil regions, the first from residues 130-170 and the second at the extreme C-terminus (residues 530-580)(43). We predict that IpaB has a similar fold to IpaD/BipD, with an internal coiled-coil, but with a much larger C-terminal domain. Due to the helical rise of the pentamer, the interface between the fifth and the first molecule is different to that between the other consecutive pairs of monomers, and therefore it is possible that the final position of the pentamer is filled by IpaB. This would explain the need for both IpaD and IpaB to properly control secretion, with four copies of IpaD polymerizing at the tip of the needle and one molecule of IpaB locking the structure.

In order to test this hypothesis, we first investigated the presence of IpaD and IpaB at the tip of the needle. Using a variety of techniques, including immunofluorescence (Supplementary Fig. 2) and EM (data not shown), we were able to observe both IpaD and IpaB at the surface of wild type *S. flexneri* (Table 2). Surface-localized IpaB was dependent on the presence of IpaD (Table 2), while IpaD was still surface-localized in the absence of IpaB(11). This suggests that IpaD is able to directly bind the MxiH needle, while IpaB requires a binding surface that involved residues on IpaD.

Based on the structure of the IpaD monomer, we designed mutants to cleanly remove the N-(41-130) and C-terminal (192-267) domains, and assessed their ability to complement an *ipaD*$^{-}$ mutant. Removal of the N-terminal domain did not affect the binding of either IpaD or IpaB at the tip of the needle, consistent with its role as a chaperone. Removal of the C-terminal domain, on the other hand, completely abolished binding of IpaB at the tip, without affecting localization of IpaD (Table 2). This is consistent with the hetero-pentamer model proposed, as

the C-terminal domain of IpaD does not contribute significantly to the IpaD-IpaD interaction (as assessed using the MSDpisa server(37)). In contrast, it would likely be involved in binding of the much larger IpaB molecule. The result, therefore, highlights an essential role for the IpaD C-terminal domain in binding the IpaB molecule. In further support of this, BipD could also be visualized on the surface of *S. flexneri* when expressed in an *ipaD*$^{-}$ mutant, but IpaB was unable to bind (Table 2).

Discussion

Here we present the first structures of T3SS needle-tip proteins from the *Shigella*/*Salmonella* family, which trigger uptake of the bacteria by non-phagocytic cells. The structures of IpaD and BipD, from *S. flexneri* and *B. pseudomallei* respectively, are homologous, consisting of a central coiled-coil with a domain at either end. The structures demonstrate the first examples of self-chaperoning within T3SS molecules and have allowed us to construct a model for a needle-tip complex of *S. flexneri*. Furthermore, we have been able to attribute different functions to distinct domains within the proteins.

IpaD has recently been shown to exist at the tip of the MxiH needle(11), from where it appears to orchestrate the correct insertion of the IpaB/C translocon into host cell membranes(9). The structures of two other needle tip proteins from distinct T3SS families are known: LcrV from *Y. pestis*(17) and EspA from *EPEC* (32). Both of these molecules also contain a central coiled-coil, but in other aspects there are few structural similarities with IpaD/BipD, especially at the N-terminus of the molecules. These structures, combined with our recent needle subunit structure(16) and the structures of the polymerizing components of the bacterial flagellum (44), serve to highlight the importance of intramolecular helical coiled-coils as scaffolds for superhelical assemblies, while emphasising that specific functions can be “bolted onto” the assembly in the form of structurally distinct domains.

Most T3SS proteins are chaperone-bound within the bacterial cytoplasm. Chaperones are thought to play multiple roles both in directing T3SS proteins to the base of the apparatus for export and also in preventing premature assembly of structural components(45). For example, EspA interacts with CesA in the bacterial cytoplasm, while LcrV seems to be chaperoned by LcrG since expression of LcrV in the absence of LcrG leads to oligomerization of LcrV(46). Although no structure of LcrG is available, the protein is predicted to be α-helical and to interact with the central coiled-coil of LcrV with 1:1 stoichiometry(46).

Based on our structural and biochemical data, we propose that the most complete models of IpaD and BipD found in our crystals represent the form of the molecule present in the bacterial cytoplasm, and that the role of the N-terminal domain is to chaperone residues on the coiled-coil involved in interactions at the tip of the needle. The proteins would be partially unfolded during export through the needle(16) and would refold at tip of the needle into an alternate conformation with the N-terminal domain pointing away from the coiled-coil. This would require that the interactions formed at the tip of the needle are more favourable than the interactions between the N-terminal domain and the coiled-coil. In this context, it is noteworthy that two structures for FliS, the closest IpaD/BipD structural homologue, have been determined that are related by opening of the four-helix bundle and rotation of one pair of helices with respect to the other (1ORJ and 1VH6) (Figure 3c).

Removal of the N-terminal domain of IpaD by proteolysis also resulted in increased flexibility of the coiled-coil. Such flexibility of the coiled-coil appears to be a common feature of needle and tip proteins and may be of importance in signalling. Our MxiH crystal structure revealed two conformations of the molecule, related by a hinging motion part way down the coiled-coil (16); while LcrV has a significant kink in its C-terminal helix(17) which matches the kink in

one of the MxiH conformations. EspA, on the other hand, contains a straight coiled-coil, as seen when it was crystallized bound to its chaperone which would likely limit the flexibility of the helices(32). By removing the N-terminal domain of IpaD we appear to have crystallographically trapped the coiled-coil in a number of states between the extremes of LcrV and EspA.

The IpaD and BipD structures represent the first examples of self-chaperoning T3SS molecules. A major question, therefore, is why they have adopted the strategy of incorporation of the chaperone into the polypeptide chain, while other T3SS filament-forming proteins maintain separate chaperones. It is tempting to speculate that fusion of the chaperone to the rest of the molecule allows for greater flexibility of function within a single polypeptide chain. Intriguingly, given the mechanism of infection employed by the *Shigella*/*Salmonella* family, three of the top five structural homologues of the N-terminal half of IpaD/BipD are proteins involved in the re-arrangement of the actin cytoskeleton. Given that *S. flexneri* secretes large amounts of IpaD upon activation, significant quantities may translocate into the host cell cytoplasm, where it would be free to refold into the bacterial cytoplasmic form and co-operate with other effector molecules in the reprogramming of the cytoskeleton. It is worth noting that a domain of SipA, an actin-binding *Salmonella* effector molecule homologous to IpaA is also a structural homologue of vinculin(47), while a recent crystal structure of vinculin bound to a helix of IpaA has demonstrated that *S. flexneri* effectors do indeed utilize molecular mimicry during infection(48).

The key role for IpaD occurs at the tip of the needle, where it is essential for mediating correct insertion of the IpaB/IpaC translocon into host cell membranes(9,11). We propose a model for an IpaD/IpaB hetero-pentamer at the tip of the MxiH needle, based on crystal contacts in one of the crystal forms. This model involves export of four copies of IpaD to the tip of the needle, where they pack into the needle via the C-terminal residues. Finally, a copy of IpaB slots into the pentamer via its central coiled-coil, thereby locking the pentamer and preventing further secretion of other effectors. This model is consistent with the helical parameters of the MxiH needle and with the published null mutant phenotypes of *S. flexneri*(8). Mutations designed based on the structure of IpaD are wholly consistent with the model and demonstrate that the C-terminal domain of IpaD is critical for binding of IpaB at the needle tip. The small amounts of effector proteins secreted in the absence of activation, termed ‘leakage’, could be explained by needles which haven't fully assembled the IpaD/IpaB plug, by premature loss of IpaD/IpaB from the tip, or by a ‘breathing’ of the structure between a closed and open state. In addition to closing the needle, this model would also position the predicted large C-terminal domain of IpaB as the most distal point from the needle, and therefore the likely point of contact with the host cell. The C-terminal domain of IpaB contains two predicted trans-membrane helices and, significantly, the top hit when searching the Protein Data Bank with its sequence (FFAS Server, (49)) is Colicin B, a bacterial pore-forming toxin which utilizes a helical trans-membrane hairpin(50). Activation of the tip complex, by contact with the host cell, could trigger a conformational change leading to an opening of the pentamer, possibly into a conformation more similar to our earlier model of LcrV at the tip(16). This would open the channel to allow export and assembly of the pore components IpaB and IpaC into the host cell membrane, thereby triggering the infectious process.

Supplementary Material

Refer to Web version on PubMed Central for supplementary material.

Acknowledgements

SJ is funded by a Medical Research Council of the UK grant (G0400389) to SML and previously by a Guy G. F. Newton Senior Research Fellowship to AB. PR is funded by a Wellcome Trust Grant (No. 077082) to SML and PR.

UKPMC Funders Group Author Manuscript

JED is funded by an Australian National Health and Medical Research Council CJ Martin Postdoctoral Fellowship (ID-358785). WDP's laboratory was supported by PHS grants AI034428 and RR017708 and the University of Kansas Research Development Fund. AB is funded by a Guy G. F. Newton Senior Research Fellowship. Work at the IAH is supported by the BBSRC (UK). Michael Wood was involved in the cloning of BipD. We are grateful to Ed Lowe, Martin Noble and Ed Mitchell for assistance with data collection and to Marc Morgan and Jenny Gibson for assistance with the crystallization robot. We are very grateful to Clemens Vonrhein for processing of the orthorhombic native data and to Tony Willis for N-terminal sequencing.

References

1. Kotloff KL, Winickoff JP, Ivanoff B, Clemens JD, Swerdlow DL, Sansonetti PJ, Adak GK, Levine MM. Bull World Health Organ 1999;77(8):651–666. [PubMed: 10516787]
2. Blocker A, Jouihri N, Larquet E, Gounon P, Ebel F, Parsot C, Sansonetti P, Allaoui A. Mol Microbiol 2001;39(3):652–663. [PubMed: 11169106]
3. Menard R, Sansonetti P, Parsot C. Embo J 1994;13(22):5293–5302. [PubMed: 7957095]
4. Blocker A, Gounon P, Larquet E, Niebuhr K, Cabiaux V, Parsot C, Sansonetti P. J Cell Biol 1999;147 (3):683–693. [PubMed: 10545510]
5. Johnson S, Deane JE, Lea SM. Curr Opin Struct Biol 2005;15(6):700–707. [PubMed: 16263265]
6. He SY, Nomura K, Whittam TS. Biochim Biophys Acta 2004;1694(13):181–206. [PubMed: 15546666]
7. Cossart P, Sansonetti PJ. Science 2004;304(5668):242–248. [PubMed: 15073367]
8. Menard R, Sansonetti PJ, Parsot C. J Bacteriol 1993;175(18):5899–5906. [PubMed: 8376337]
9. Picking WL, Nishioka H, Hearn PD, Baxter MA, Harrington AT, Blocker A, Picking WD. Infect Immun 2005;73(3):1432–1440. [PubMed: 15731041]
10. Blocker A, Komoriya K, Aizawa S. Proc Natl Acad Sci U S A 2003;100(6):3027–3030. [PubMed: 12631703]
11. Espina M, Olive AJ, Kenjale R, Moore DS, Ausar SF, Kaminski RW, Oaks EV, Middaugh CR, Picking WD, Picking WL. Infect Immun 2006;74(8):4391–4400. [PubMed: 16861624]
12. Mueller CA, Broz P, Muller SA, Ringler P, Erne-Brand F, Sorg I, Kuhn M, Engel A, Cornelis GR. Science 2005;310(5748):674–676. [PubMed: 16254184]
13. White NJ. Lancet 2003;361(9370):1715–1722. [PubMed: 12767750]
14. Stevens MP, Haque A, Atkins T, Hill J, Wood MW, Easton A, Nelson M, Underwood-Fowler C, Titball RW, Bancroft GJ, Galyov EE. Microbiology 2004;150(Pt 8):2669–2676. [PubMed: 15289563]
15. Cordes FS, Komoriya K, Larquet E, Yang S, Egelman EH, Blocker A, Lea SM. J Biol Chem 2003;278 (19):17103–17107. [PubMed: 12571230]
16. Deane JE, Roversi P, Cordes FS, Johnson S, Kenjale R, Daniell S, Booy F, Picking WD, Picking WL, Blocker AJ, Lea SM. Proc Natl Acad Sci USA 2006;103:12529–12533. [PubMed: 16888041]
17. Derewenda U, Mateja A, Devedjiev Y, Routzahn KM, Evdokimov AG, Derewenda ZS, Waugh DS. Structure (Camb) 2004;12(2):301–306. [PubMed: 14962390]
18. Johnson S, Roversi P, Espina M, Deane JE, Birket S, Picking WD, Blocker A, Picking WL, Lea SM. Acta Crystallograph Sect F Struct Biol Cryst Commun 2006;62:865–8.
19. Schneider TR, Sheldrick GM. Acta Crystallogr D Biol Crystallogr 2002;58(Pt 10 Pt 2):1772–1779. [PubMed: 12351820]
20. Vonrhein, C.; Blanc, E.; Roversi, P.; Bricogne, G. Automated Structure Solution with autoSHARP. In: Doublie, S., editor. Crystallographic Methods. Humana Press; 2005.
21. de La Fortelle E, Bricogne G. Methods in Enzymology 1997;276:472–494.
22. Terwilliger TC. Methods Enzymol 2003;374:22–37. [PubMed: 14696367]
23. CCP4. Acta Crystallographica 1994;D50:760–763.
24. McRee DE. J Struct Biol 1999;125(23):156–165. [PubMed: 10222271]
25. Blanc E, Roversi P, Vonrhein C, Flensburg C, Lea SM, Bricogne G. Acta Crystallogr D Biol Crystallogr 2004;60(Pt 12 Pt 1):2210–2221. [PubMed: 15572774]
26. DeLano, WL. 2002. http://www.pymol.org

27. Roversi P, Johnson S, Field T, Deane JE, Galyov EE, Lea SM. Acta Crystallograph Sect F Struct Biol Cryst Commun 2006;62:861–4.
28. Holm L, Sander C. J Mol Biol 1993;233(1):123–138. [PubMed: 8377180]
29. Thompson JD, Higgins DG, Gibson TJ. Nucleic Acids Res 1994;22(22):4673–4680. [PubMed: 7984417]
30. Gouet P, Courcelle E, Stuart DI, Metoz F. Bioinformatics 1999;15(4):305–308. [PubMed: 10320398]
31. Pope LM, Reed KE, Payne SM. Infect Immun 1995;63(9):3642–3648. [PubMed: 7642302]
32. Yip CK, Finlay BB, Strynadka NC. Nat Struct Mol Biol 2005;12(1):75–81. [PubMed: 15619638]
33. Aizawa SI, Vonderviszt F, Ishima R, Akasaka K. J Mol Biol 1990;211(4):673–677. [PubMed: 2313691]
34. Evdokimov AG, Phan J, Tropea JE, Routzahn KM, Peters HK, Pokross M, Waugh DS. Nat Struct Biol 2003;10(10):789–793. [PubMed: 12958592]
35. Phan J, Austin BP, Waugh DS. Protein Sci 2005;14(10):2759–2763. [PubMed: 16195558]
36. Espina M, Ausar SF, Middaugh CR, Picking WD, Picking WL. Biochemistry 2006;45(30):9219–9227. [PubMed: 16866368]
37. Krissinel, E.; Henrick, K. Detection of Protein Assemblies in Crystals. In: Berthold, MR., editor. Lecture Notes in Computer Science. Springer Berlin / Heidelberg; 2005.
38. Papagrigoriou E, Gingras AR, Barsukov IL, Bate N, Fillingham IJ, Patel B, Frank R, Ziegler WH, Roberts GC, Critchley DR, Emsley J. Embo J 2004;23(15):2942–2951. [PubMed: 15272303]
39. Izard T, Evans G, Borgon RA, Rush CL, Bricogne G, Bois PR. Nature 2004;427(6970):171–175. [PubMed: 14702644]
40. Pokutta S, Weis WI. Mol Cell 2000;5(3):533–543. [PubMed: 10882138]
41. Venkatesan MM, Buysse JM, Oaks EV. J Bacteriol 1992;174(6):1990–2001. [PubMed: 1312536]
42. West NP, Sansonetti P, Mounier J, Exley RM, Parsot C, Guadagnini S, Prevost MC, Prochnicka-Chalufour A, Delepierre M, Tanguy M, Tang CM. Science 2005;307(5713):1313–1317. [PubMed: 15731456]
43. Lupas A. Prediction and Analysis of Coiled-Coil Structures. 1996
44. Yonekura K, Maki-Yonekura S, Namba K. Nature 2003;424(6949):643–650. [PubMed: 12904785]
45. Parsot C, Hamiaux C, Page AL. Curr Opin Microbiol 2003;6(1):7–14. [PubMed: 12615213]
46. Lawton DG, Longstaff C, Wallace BA, Hill J, Leary SE, Titball RW, Brown KA. J Biol Chem 2002;277(41):38714–38722. [PubMed: 12107165]
47. Lilic M, Vujanac M, Stebbins CE. Mol Cell 2006;21(5):653–664. [PubMed: 16507363]
48. Hamiaux C, van Eerde A, Parsot C, Broos J, Dijkstra BW. EMBO Rep. 2006
49. Jaroszewski L, Rychlewski L, Li Z, Li W, Godzik A. Nucleic Acids Res 2005;33:W284–288. [PubMed: 15980471]Web Server issue
50. Hilsenbeck JL, Park H, Chen G, Youn B, Postle K, Kang C. Mol Microbiol 2004;51(3):711–720. [PubMed: 14731273]

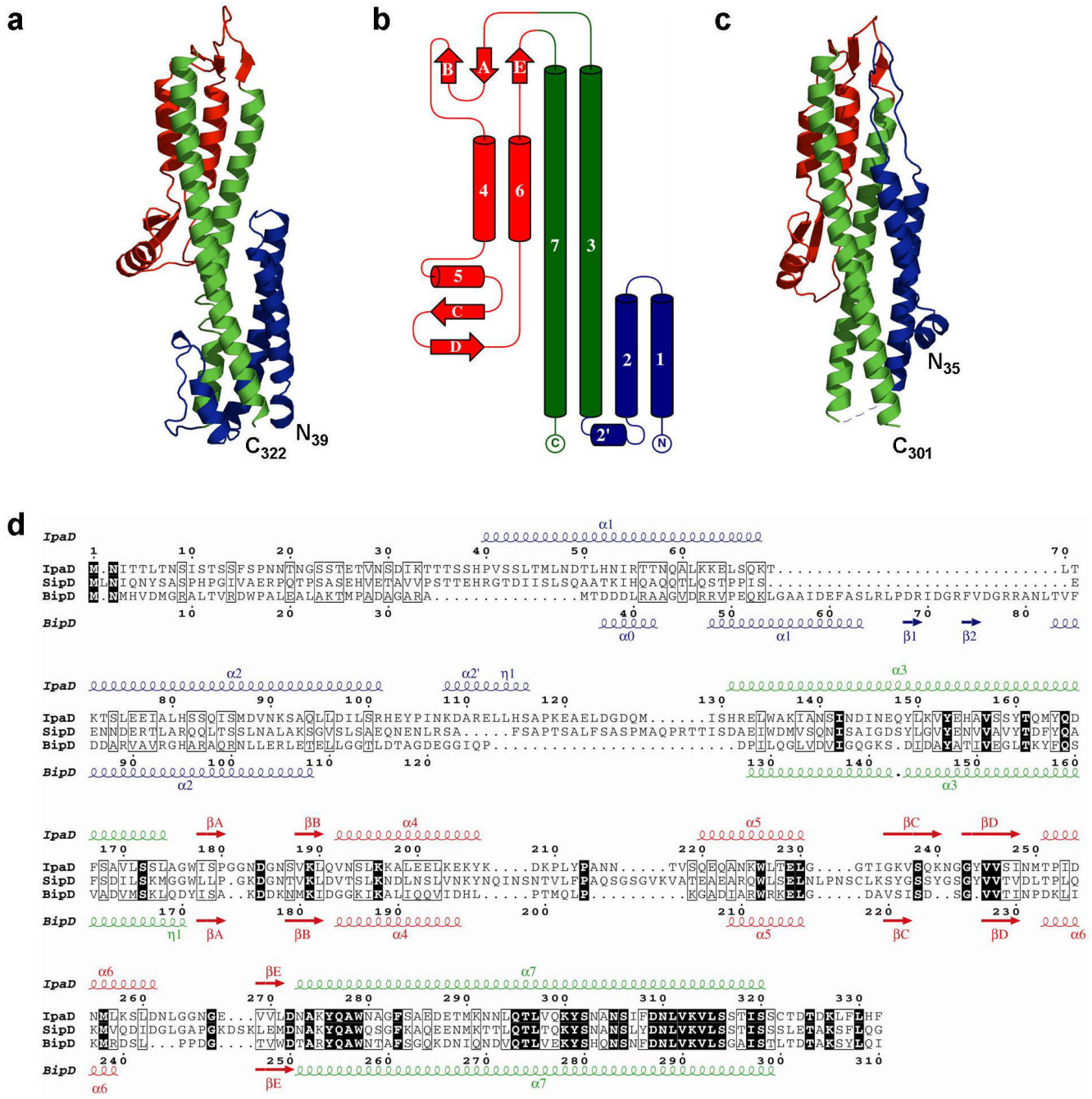

Figure 1.

Crystal structures of IpaD and BipD.**(a)** Ribbon diagram of the structure of IpaD (residues 39-322) colored by domain; N-domain (blue), central coiled-coil (green), C-domain (red). **(b)** Topology diagram of IpaD, colored as in (a). **(c)** Structure of BipD (residues 35-111 and 127-301) colored as in **a**. All figures produced using PyMOL(26). **(d)** Structure based sequence alignment of IpaD, SipD and BipD using the ESPript server(30), colored according to residue conservation. Secondary structure elements of IpaD and BipD are shown above and below the alignment respectively. The *Salmonella enterica typhimurium* homologue SipD is more closely related to IpaD.

UKPMC Funders Group Author Manuscript

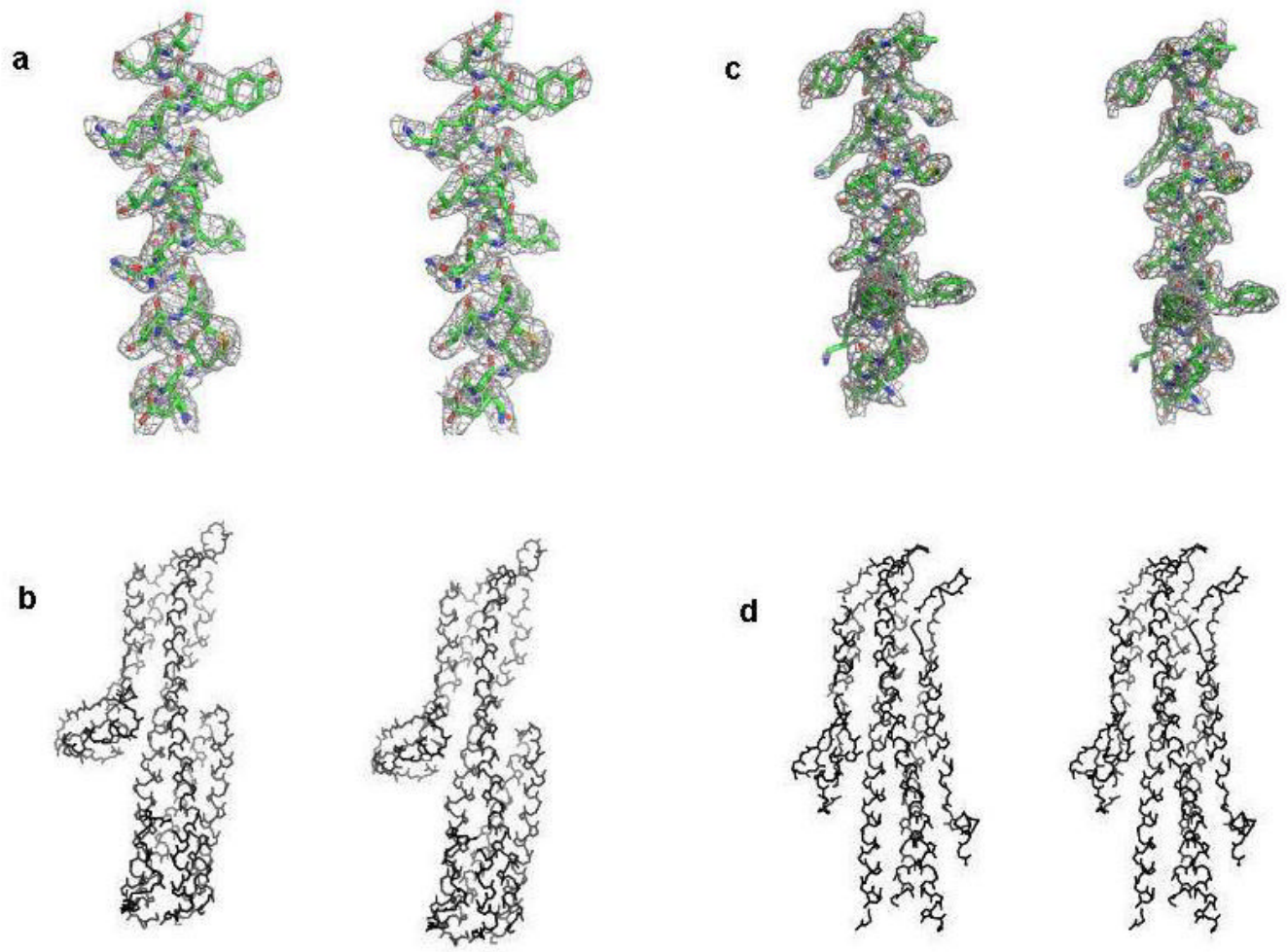

Figure 2.

Stereo views of IpaD and BipD electron density (**a** and **c**) and main chain traces (**b** and **d**) are shown. The electron density is calculated with coefficients $2F_O$-wF_C and phases derived from the final models. The IpaD density in panel (**a**) is contoured at 1.0 σ around residues 284-304 in the C-terminal coiled-coil helix and the BipD density in (**c**) around residues 154-172 in the N-terminal coiled-coil helix. (**b**) and (**d**) show complete main chain traces oriented so that the N- and C-termini are at the bottom of the picture.

UKPMC Funders Group Author Manuscript

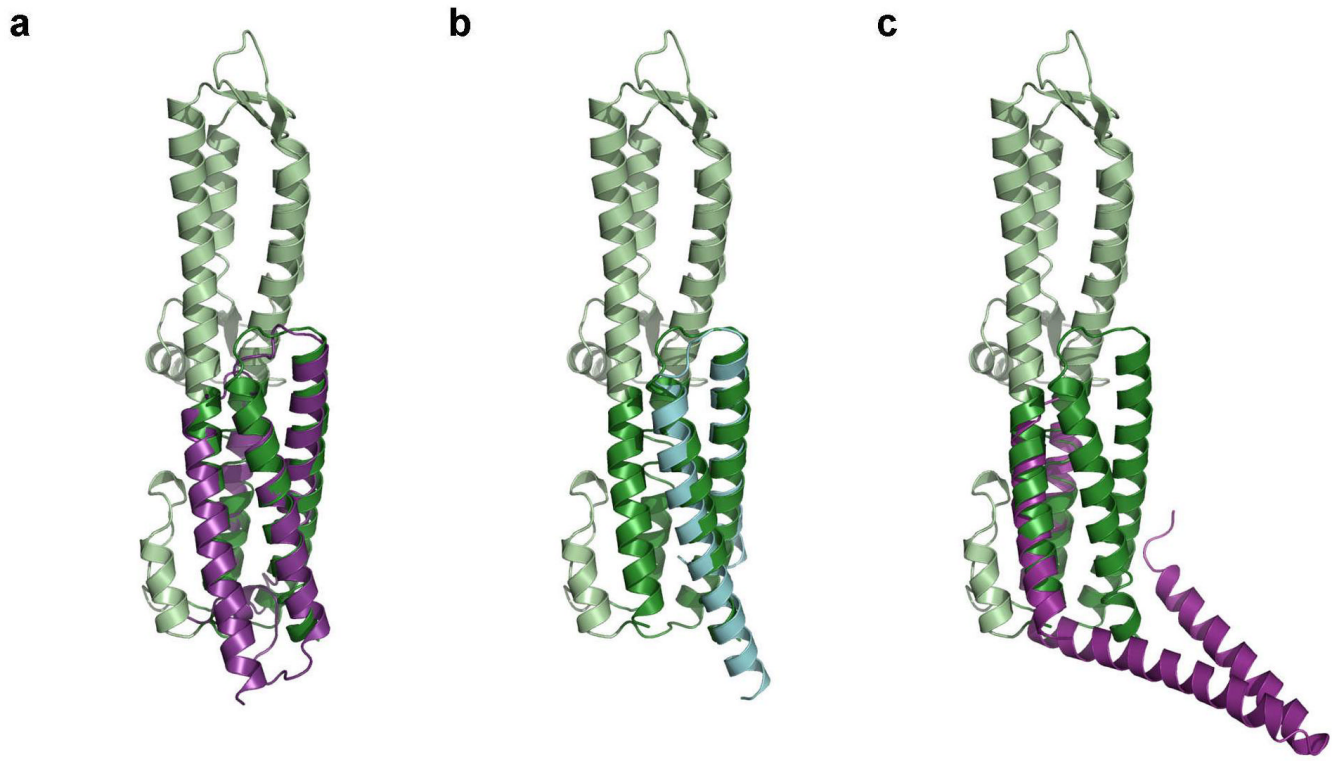

Figure 3.

The N-terminal domain is a chaperone. **(a)** Ribbon diagram of IpaD (green) superposed on *Aquifex aeolicus* FliS (purple, 1ORJ-A, (rmsd = 2.0 Å over 103 Cα atoms)(39). **(b)** Ribbon diagram of IpaD (green) superposed on *Yersinia pestis* YscE (light blue, 1ZW0-A, rmsd = 1.8 Å over 57 Cα atoms)(35). **(c)** Ribbon diagram of IpaD (green) superposed on *Bacillus subtilis* FliS (purple, 1VH6) demonstrating the opened four-helix bundle.

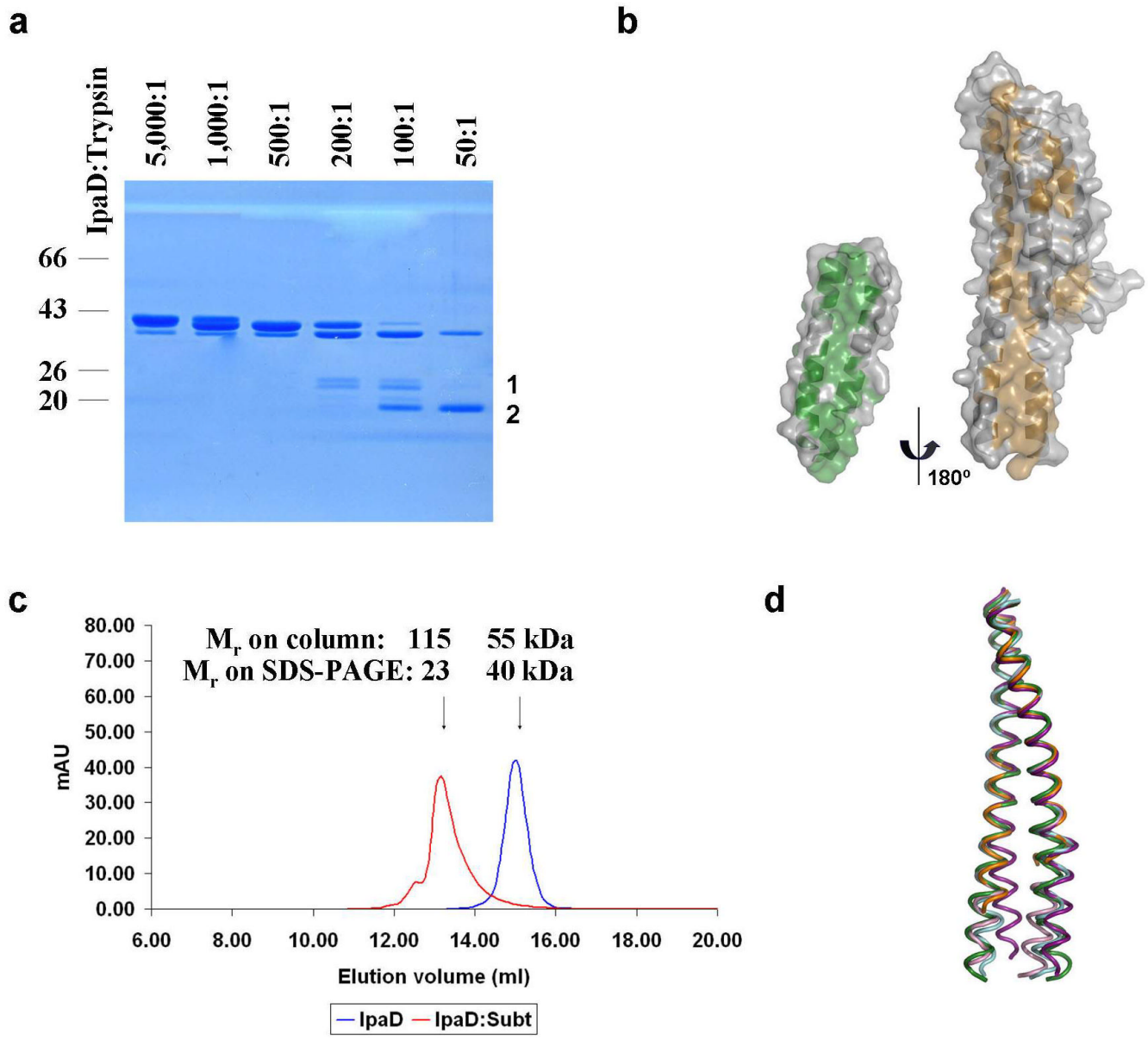

Figure 4.

Consequences of removal of the N-terminal domain. **(a)** Proteolytic sensitivity of the N-terminal domain of IpaD. IpaD was incubated with trypsin at various ratios (w:w) and the resulting digests were resolved on SDS-PAGE. Band 1 (24 kDa) begins at residue 120 and Band 2 (20 kDa) at residue 138. **(b)** Surface representation of $IpaD_{39\text{-}130}$ (left) and $IpaD_{131\text{-}322}$ (right) with hydrophobic residues colored green and brown respectively. $IpaD_{39\text{-}130}$ is rotated through 180° along the long axis relative to $IpaD_{131\text{-}322}$ in order to demonstrate the complementary hydrophobic surfaces. The surface is presented as transparent to allow visualization of the secondary structure. **(c)** Analytical gel filtration chromatography (Superdex 200, HR 10/30) of IpaD before and after Subtilisin treatment. Elution volume of each species is noted along with the M_r calculated from SDS-PAGE. **(d)** Overlay of 5 structures of the IpaD coiled-coil demonstrating the flexibility of the helices in the absence of the N-terminal domain. The conformation of the coil in the presence of the N-terminal domain is shown in green. The C-terminal domain has been removed to aid clarity.

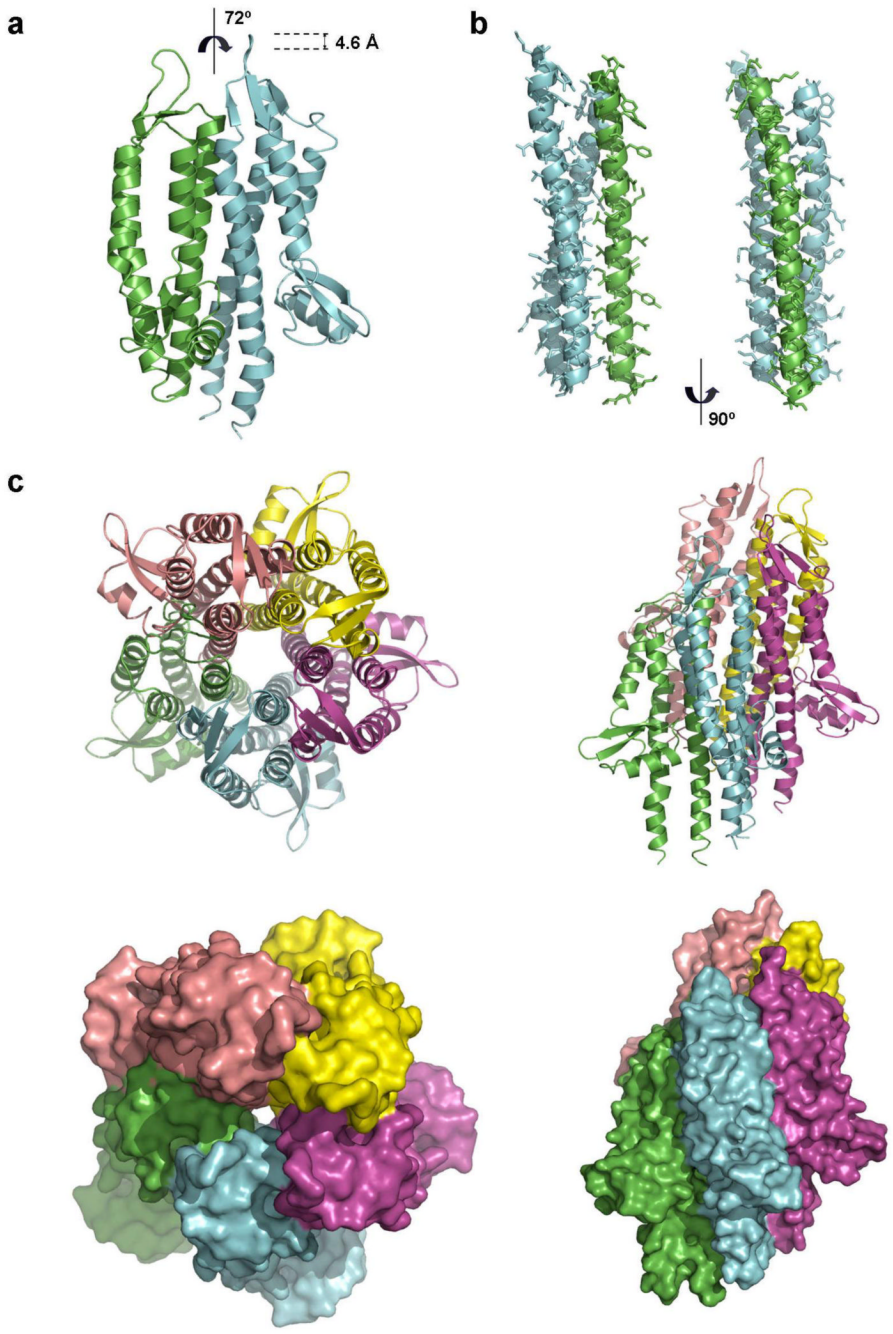

Figure 5.

Oligomerization of IpaD. **(a)** Ribbon diagram of the non-crystallographic dimer found in crystal form 2 (18). Molecule A is shown in green, molecule B in blue. **(b)** Detailed view of the dimer interaction site with sidechains displayed, colored as in **a.** Only structural elements that contribute to the binding site are displayed for clarity. **c)** Pentamer produced using the non-crystallographic symmetry from crystal form 2. At the top are ribbon representations and at the bottom surface views. The panels on the left are related to the panels on the right by a rotation of 90°.

UKPMC Funders Group Author Manuscript

Table 1

IpaD and BipD refinements statistics (program Buster-TNT)

Values for the highest resolution shell are given in parentheses

Crystal	**IpaD CF-1**	**IpaD CF-2**	**IpaD CF-4**	**BipD CF-1**	**BipD CF-2**
Space Group (Z)	P212121 (8)	C2 (8)	C2 (8)	P21212 (8)	C222 (8)
Cell Parameters (Å)	a=55.9, b=100.7, c=112.0	a=77.9, b=91.5, c=54.9 β=96.4°	a=137.8, b=44.5, c=100.3 β=108.0°	a=136.5, b=89.8, c=50.2	a=104.0, b=122.8, c=49.2
Resolution range (Å)	20.0-3.0(3.1-3.0)	15.0-2.1(2.2-2.1)	34.0-3.2(3.3-3.2)	54.0-2.7(2.9-2.7)	40.0-2.6(2.8-2.6)
Unique reflections	12157	22218	9791	17569	10013
R(%)	0.237(0.276)	0.190(0.208)	0.248(0.257)	0.218(0.253)	0.206(0.226)
Rwork (%)	0.235(0.271)	0.189(0.207)	0.247(0.252)	0.216(0.251)	0.203(0.224)
Rfree (%)	0.271(0.376)	0.216(0.229)	0.274(0.337)	0.259(0.288)	0.245(0.263)
Rmsd bond lengths (Å)	0.002	0.007	0.010	0.003	0.005
Rmsd bond angles (°)	0.59	1.22	1.2	0.78	0.42
Residues modelled (range)	A,B: 39-322	A: 144-314 B:133-319	A:124-177; 183-322 B:123-328	A: 35-111; 127-301 B: 35-111; 125-301	A: 34-111; 125-302
Waters modeled	21	208	8	44	50
Non-protein molecules	1 glycerol	-	-	1 citrate	-
PDB identifier	2j0o	2j0n		2cmq	2ixr

Table 2

Needle-tip localization of IpaD and IpaB

	Wild type	*ipaD*$^{-}$	*ipaD*$^{-}$/ IpaD$_{\Delta 41\text{-}130}$	*ipaD*$^{-}$/ IpaD$_{\Delta 192\text{-}267}$	*ipaD*$^{-}$/ BipD
IpaD/BipD at needle-tip	+	–	+	+	+
IpaB at needle-tip	+	–	+	–	–